January 2015

Thermal and electromechanical properties of melilite-type piezoelectric single crystals

Chuanying Shen
Shandong University

Shujun Zhang
Pennsylvania State University, shujun@uow.edu.au

Wenwu Cao
Pennsylvania State University

Hengjiang Cong
Shandong University

Haohai Yu
Shandong University

See next page for additional authors

Thermal and electromechanical properties of melilite-type piezoelectric single crystals

Abstract

Melilite-type crystals, including Ca2Ga2SiO7, Ca2MgSi2O7, and CaNdGa3O7, were successfully grown by the Czochralski technique. Thermal properties were investigated and full matrices of electromechanical constants of these melilite crystals were evaluated by impedance method, with d14 being on the order of 5.3-9.3 pC/N. The relationship between microstructure and electromechanical properties of the three kinds of crystals was established, in order to explore the piezoelectric origin and further optimize the piezoelectric properties. The distortion of eight-fold antiprisms and the distortion/rotation of tetrahedrons were thought to contribute to the piezoelectric d14 and d36, respectively. In addition, the layered structure leads to strong anisotropic behavior, accounts for the high resistivity along Z direction in Ca2MgSi2O7, while the disordered structure accounts for the degraded resistivity in CaNdGa3O7. The properties at elevated temperature were investigated, where the elastic constants show high thermal stability over the range of 25-500 C, with minimal variation of 6%.

Publication Details

Shen, C., Zhang, S., Cao, W., Cong, H., Yu, H., Wang, J. & Zhang, H. (2015). Thermal and electromechanical properties of melilite-type piezoelectric single crystals. Journal Of Applied Physics, 117 (6), 064106-1-064106-7.

Authors

Chuanying Shen, Shujun Zhang, Wenwu Cao, Hengjiang Cong, Haohai Yu, Jiyang Wang, and Huaijin Zhang

Thermal and electromechanical properties of melilite-type piezoelectric single crystals

Chuanying Shen,[1,2] Shujun Zhang,[2,a)] Wenwu Cao,[2] Hengjiang Cong,[1] Haohai Yu,[1] Jiyang Wang,[1] and Huaijin Zhang[1,b)]
[1]*State Key Laboratory of Crystal Materials, Institute of Crystal Materials, Shandong University, Jinan, Shandong 250100, China*
[2]*Materials Research Institute, Pennsylvania State University, University Park, Pennsylvania 16802, USA*

(Received 2 December 2014; accepted 2 February 2015; published online 11 February 2015)

Melilite-type crystals, including $Ca_2Ga_2SiO_7$, $Ca_2MgSi_2O_7$, and $CaNdGa_3O_7$, were successfully grown by the Czochralski technique. Thermal properties were investigated and full matrices of electromechanical constants of these melilite crystals were evaluated by impedance method, with d_{14} being on the order of 5.3–9.3 pC/N. The relationship between microstructure and electromechanical properties of the three kinds of crystals was established, in order to explore the piezoelectric origin and further optimize the piezoelectric properties. The distortion of eight-fold antiprisms and the distortion/rotation of tetrahedrons were thought to contribute to the piezoelectric d_{14} and d_{36}, respectively. In addition, the layered structure leads to strong anisotropic behavior, accounts for the high resistivity along Z direction in $Ca_2MgSi_2O_7$, while the disordered structure accounts for the degraded resistivity in $CaNdGa_3O_7$. The properties at elevated temperature were investigated, where the elastic constants show high thermal stability over the range of 25–500 °C, with minimal variation of 6%. © *2015 AIP Publishing LLC*. [http://dx.doi.org/10.1063/1.4908113]

I. INTRODUCTION

Mineral melilites have been found in meteorites, blast furnace slags, igneous, and metamorphic rocks.[1] Melilites were also found in industrial slag and clinkers and are important component in technological glasses.[2] Melilite-family compounds exhibit a general formula $(A_1A_2)_2\{(B_1B_2)(C_1C_2)\}_3O_7$, where A, B, and C denote three distinct cationic sites, and the largest A site is a distorted eight-fold coordinated antiprism being occupied by divalent cation A_1 (Ca, Sr, Ba, etc.) and/or trivalent A_2 (La, Nd, Pr, etc.); the smaller site B is regular tetrahedral, which is occupied by divalent B_1 (Mg, Zn) and/or trivalent B_2 cation (Al, Ga); the smallest site C is a distorted tetrahedral, where trivalent C_1 cation (Al, Ga) and/or tetravalent C_2 cation (Si, Ge) occupy this position.[3,4] Melilite belongs to a tetragonal system with space group of $\bar{4}2_1m$,[5,6] the structure was firstly determined by Warren,[7] and subsequently refined by Smith[8] and Bindi *et al.*[9]

Melilite crystals with a wide range of chemical compositions can be easily grown by Czochralski method, attracted attentions from scientists and engineers in the last decades. Much effort has been dedicated to the crystal growth and piezoelectric investigations.[10–14] It was reported that the piezoelectric coefficient d_{14} varied a lot for different melilite crystals ($Ca_2MgSi_2O_7$ (CMS), $d_{14} = 3.2$ pC/N;[10] $Ca_2Al_2SiO_7$, $d_{14} = 6.0$ pC/N;[11,12] and $SrGdGa_3O_7$, $d_{14} = 14.5$pC/N (Refs. 13 and 14)). Thus, it is interesting to explore the origin of piezoelectric properties based on the microstructure. In this work, $Ca_2Ga_2SiO_7$ (CGS), $Ca_2MgSi_2O_7$, and $CaNdGa_3O_7$ (CNG) were grown by the Czochralski technique. The complete set of dielectric, elastic, piezoelectric constants, and electromechanical coupling factors were determined. The relationship between microstructure and electromechanical properties of these melilite crystals were compared and discussed in relation to the tetrahedral layers and eight-fold antiprisms structure, the piezoelectric origin was studied, which will benefit the optimization of the piezoelectric properties in melilite crystals. Furthermore, the temperature dependent of electromechanical properties was investigated.

II. EXPERIMENTAL DETAILS

A. Crystal growth and structure analysis

The raw materials for CGS, CMS, and CNG, including high-purity reagents $CaCO_3$, SiO_2, Ga_2O_3, Nd_2O_3, and MgO, were weighed according to stoichiometric amounts to synthesize the polycrystalline compounds. Excess of Ga_2O_3 (1% of the total mass) was added to compensate for the evaporation during the growth process. Crystals were grown by the RF-heating Czochralski technique in an atmosphere of nitrogen (to suppress volatilization of Ga_2O_3 during the growth process) containing 2 vol. % oxygen using iridium crucible. An [001]-oriented $Ca_2Ga_2SiO_7$ crystal seed was lowered to a position slightly above the melt surface and wait until reaching thermal equilibrium, then slowly introduced into the melt. To prevent dislocations in the seed and get high quality single crystals, the necking process is important. The crystal was pulled at a speed of 0.5–1.0 mm/h with a rotation rate of 10–30 rpm. After the growth process, the grown crystal was cooled down to room temperature at a rate of 10–30 °C/h to avoid cracking caused by the anisotropic thermal stress. The growth processes of CMS and CNG crystals are similar to that of CGS crystal.

a)Electronic mail: soz1@psu.edu
b)Electronic mail: huaijinzhang@sdu.edu.cn

The structure, atomic coordinate locations, and bond lengths of the as-grown crystals were determined and refined by X-ray powder diffraction (XRD) using Jade10 software.

B. Thermal properties

The specific heat was measured using a simultaneous thermal analyzer (Perkin Elmer Diamond: DSC). Crystal samples with dimensions of $5 \times 6 \times 7\,\text{mm}^3$ were used to determine the thermal expansion coefficients using a thermal mechanical analyzer (PerkinElmer model: Diamond TMA).

C. Electromechanical properties

Melilite crystals with $\bar{4}2m$ space group possess ten non-zero independent electromechanical constants, including two dielectric permittivities ε_{11} and ε_{33}; six elastic compliances s_{11}, s_{12}, s_{13}, s_{33}, s_{44}, and s_{66}; and two piezoelectric coefficients d_{14} and d_{36}. Different geometry specimens were made based on the IEEE Standards on Piezoelectricity[15] for electromechanical constants determination, as shown in Figure 1. The dimensions of the specimens were $8 \times 8 \times 2\,\text{mm}^3$ for the *X*- and *Z*-cut square plates and $12 \times 4 \times 2\,\text{mm}^3$ for the long bars. All specimens were vacuum-sputtered Pt thin films (200 nm) on the parallel large faces as electrodes.

The dielectric constants were determined from capacitances measured using a high precision LCR meter (Agilent HP 4184A) at 100 Hz–100 kHz. The resonance and anti-resonance frequencies used to calculate the elastic constants and electromechanical coupling factors were measured using an Agilent HP 4194A impedance/gain-phase analyzer. The electrical resistivities (above 300 °C) were determined by measuring the currents of X- and Z-plates under an applied voltage of ±100 V, using a source meter (Keithley 2410C, MetricTest, Hayward, CA).

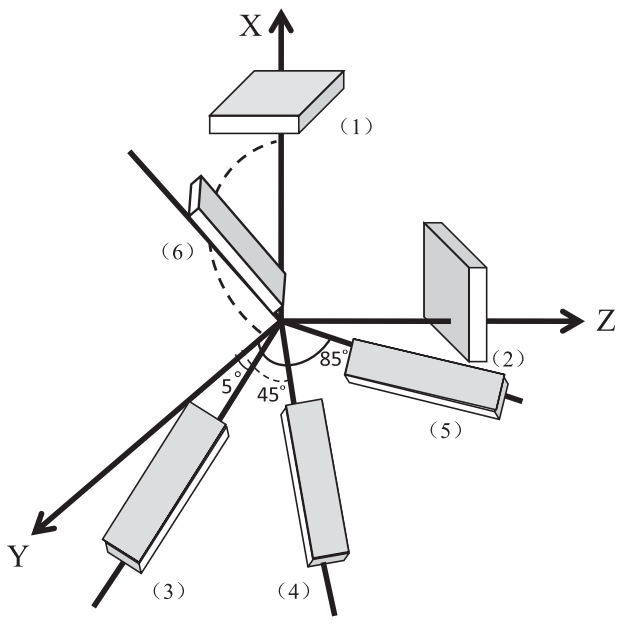

FIG. 1. Schematic of specimens: (1) *X*-cut; (2) *Z*-cut; (3) *xyt*5°; (4) *xyt*45°; (5) *xy*85°; and (6) *zxt*45°.

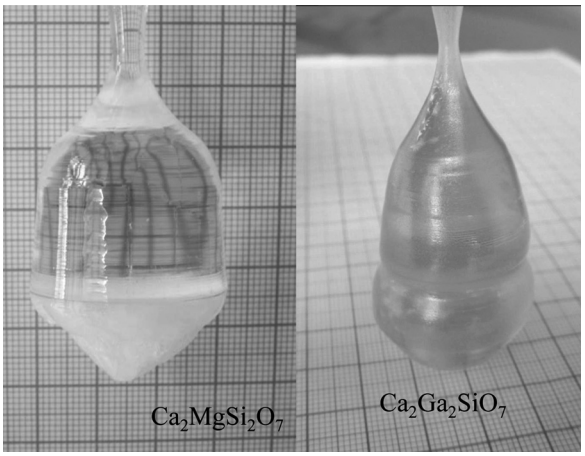

FIG. 2. The as-grown $Ca_2Ga_2SiO_7$ and $Ca_2MgSi_2O_7$ crystals pulled along [001]-direction.

III. RESULTS AND DISCUSSION

A. Crystal growth and structural analysis

Figure 2 shows the as-grown $Ca_2Ga_2SiO_7$ and $Ca_2MgSi_2O_7$ crystals pulled along [001]-direction. X-ray powder diffraction showing the as-grown crystals consists of a single phase belonging to the $P\bar{4}2_1m$ space group. The structure of $Ca_2Ga_2SiO_7$ was given in Figure 3, from which, regular GaO_4 tetrahedrons and corner-sharing irregular tetrahedrons (GaO_4/SiO_4) forming the tetrahedral layers (GaO_4 and SiO_4 tetrahedrons linked each other forming five-membered rings) in the *XY* plane, while the layers are linked

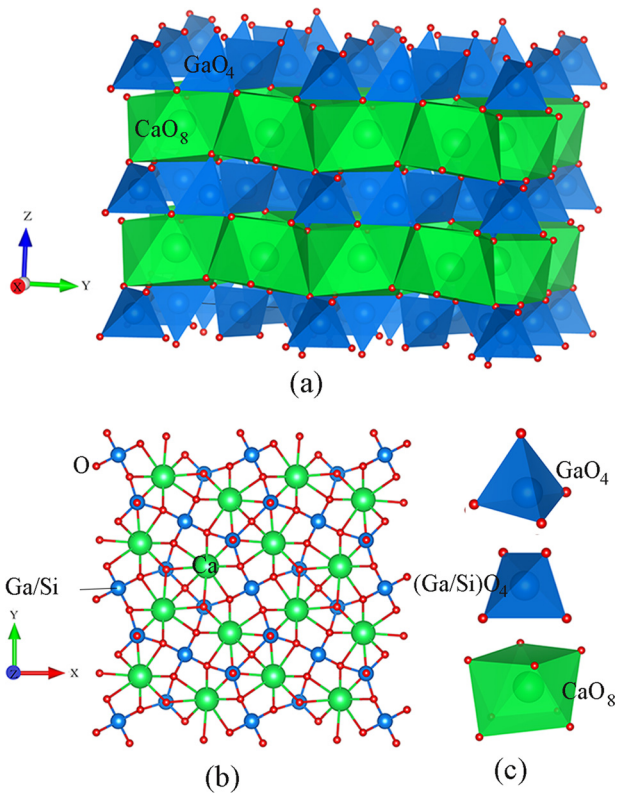

FIG. 3. Projection of the average crystal structure of $Ca_2Ga_2SiO_7$ (a) projected along *X*-direction, (b) projected along *Z*-direction, and (c) GaO_4/SiO_4 tetrahedrons and CaO_8 antiprism.

together along the Z-axis by Ca cations on eight-fold coordinate sites. The structure of $Ca_2MgSi_2O_7$ crystal is similar to that of $Ca_2Ga_2SiO_7$, where the Mg^{2+} ions are located at regular tetrahedral positions, while Si^{4+} ions are located at irregular tetrahedral positions. Similarly, $CaNdGa_3O_7$ crystals were found to possess the same structure, where Ca^{2+} and Nd^{3+} ions (distributed randomly with a ratio of 1:1) are located at the eight-fold coordinate antiprisms, while Ga^{3+} cations are located at tetrahedral positions.

B. Thermal properties

The temperature dependence of specific heat (C_p) for $Ca_2Ga_2SiO_7$ and $Ca_2MgSi_2O_7$ crystals is shown in Figure 4. One can see that the specific heat of $Ca_2Ga_2SiO_7$ increases linearly from 0.629 $J\cdot g^{-1}\cdot {}^\circ C^{-1}$ to 0.985 $J\cdot g^{-1}\cdot {}^\circ C^{-1}$ over the temperature range of 20–300 °C. A small peak was observed at 87 °C for $Ca_2MgSi_2O_7$ crystals, which is associated with the incommensurate-normal phase transition,[16] above which, the specific heat was found to increase linearly from 0.889 $J\cdot g^{-1}\cdot {}^\circ C^{-1}$ to 1.120 $J\cdot g^{-1}\cdot {}^\circ C^{-1}$. The specific heat of CNG is smaller than those of CMS and CGS, increasing linearly from 0.456 $J\cdot g^{-1}\cdot {}^\circ C^{-1}$ to 0.598 J/g·°C over the same temperature range.

Figure 5 presents the temperature dependence of thermal expansions for (a) CGS and (b) CMS crystals. From Figure 5(a), the thermal expansions were found to increase slightly with temperature for CGS over the temperature range of 25–500 °C with average thermal expansion coefficients of $5.7\times10^{-6}/{}^\circ C$ and $8.7\times10^{-6}/{}^\circ C$ along the *X*- and *Z*-directions, respectively. For CMS, the thermal expansion along *X*-direction was found to increase linearly over the studied temperature range, while for *Z*-direction, it decreases in the range of 25–87 °C, then increases slightly up to 500 °C, with the inversion point being associated with the incommensurate-normal transition temperature.[17] Above 87 °C, the average thermal expansion coefficients were calculated to be $8.0\times10^{-6}/{}^\circ C$ and $8.8\times10^{-6}/{}^\circ C$ along *X*- and *Z*-directions, showing minimal variation; whereas for CNG, they are $5.4\times10^{-6}/{}^\circ C$ and $6.6\times10^{-6}/{}^\circ C$, respectively.

Using the Archimedes method, the densities of CGS and CMS at room temperature were measured to be 3.795 g/cm^3 and 2.960 g/cm^3, respectively. The density at different temperatures can be evaluated based on the thermal expansion curves, as shown in the inset of Figure 5. Over the temperature range of 25–500 °C, the densities of CGS, CMS, and CNG were found to decrease linearly from 3.795 g/cm^3 to 3.790 g/cm^3, from 2.960 g/cm^3 to 2.946 g/cm^3, and from 5.139 g/cm^3 to 5.097 g/cm^3, respectively.

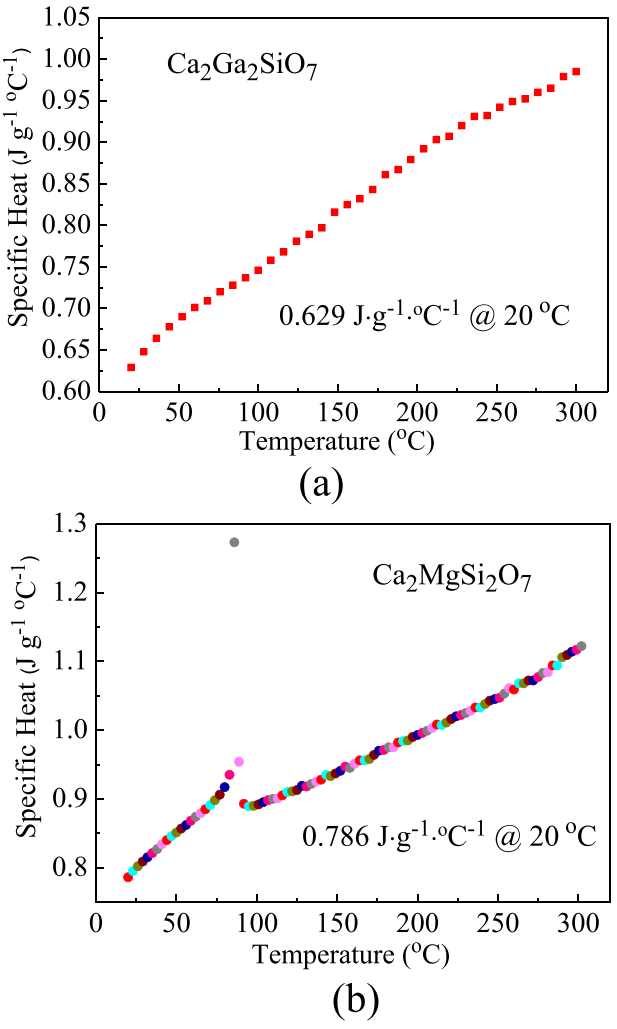

FIG. 4. The specific heat of (a) $Ca_2Ga_2SiO_7$ and (b) $Ca_2MgSi_2O_7$ crystals as a function of temperature.

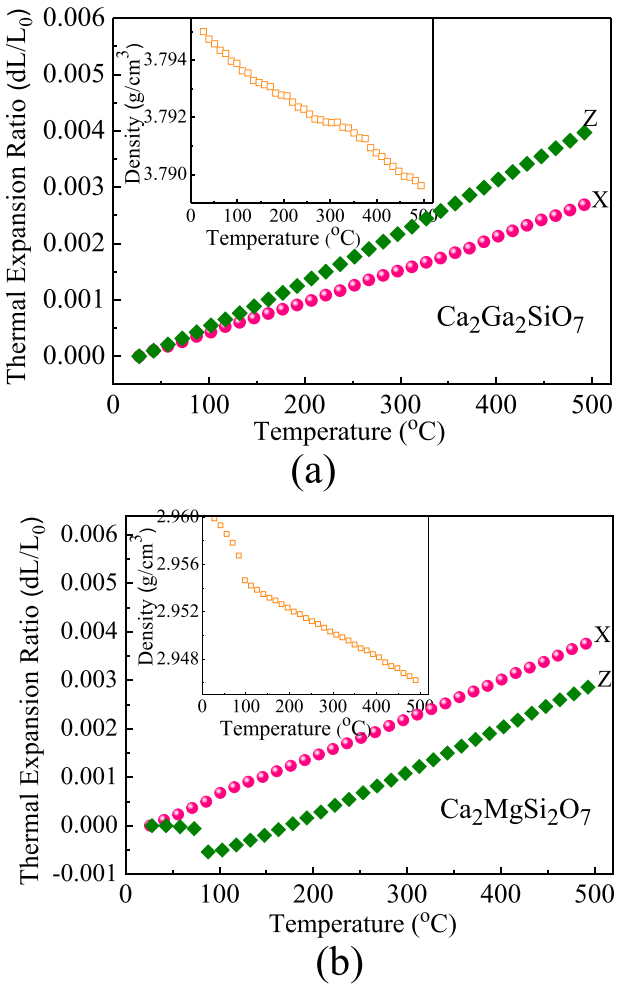

FIG. 5. The thermal expansions of (a) $Ca_2Ga_2SiO_7$ and (b) $Ca_2MgSi_2O_7$ as a function of temperature.

TABLE I. The room temperature electromechanical constants of melilite crystals.

Crystals	$\varepsilon_{11}^T/\varepsilon_0$	$\varepsilon_{33}^T/\varepsilon_0$
	Dielectric constants $\varepsilon_{ii}^T/\varepsilon_0$	
$CaNdGa_3O_7$ (Ref. 18)	16.8	10.9
$Ca_2Ga_2SiO_7$	12.6	7.4
$Ca_2MgSi_2O_7$	11.7	8.0

	s_{11}^E	s_{12}^E	s_{13}^E	s_{33}^E	s_{44}^E	s_{66}^E
	Elastic compliance constants s_{ij} (pm^2/N)					
$CaNdGa_3O_7$ (Ref. 18)	8.5	−3.5	−1.9	6.8	26.0	16.5
$Ca_2Ga_2SiO_7$	8.2	−3.3	−1.9	8.1	31.1	15.0
$Ca_2MgSi_2O_7$	9.0	−4.4	−2.0	8.4	33.6	18.6

	c_{11}^E	c_{12}^E	c_{13}^E	c_{33}^E	c_{44}^E	c_{66}^E
	Elastic stiffness constants c_{ij} (10^{10} N/m^2)					
$CaNdGa_3O_7$ (Ref. 18)	16.9	8.5	7.1	18.7	3.8	6.1
$Ca_2Ga_2SiO_7$	16.8	8.1	5.9	15.1	3.2	6.7
$Ca_2MgSi_2O_7$	17.5	10.0	6.6	15.1	3.0	5.4

	d_{14}	d_{36}	e_{14}	e_{36}
	Piezoelectric coefficients d_{ij} (pC/N) and e_{ij} (C/m^2)			
$CaNdGa_3O_7$ (Ref. 18)	9.3	1.7	0.36	0.10
$Ca_2Ga_2SiO_7$	6.4	1.4	0.21	0.09
$Ca_2MgSi_2O_7$	5.3	4.3	0.16	0.23

	k_{14}	k_{36}
	Electromechanical coupling factors k_{ij} (%)	
$CaNdGa_3O_7$ (Ref. 18)	14.9	4.2
$Ca_2Ga_2SiO_7$	10.9	4.5
$Ca_2MgSi_2O_7$	8.0	8.3

C. Room temperature electromechanical properties

Table I lists the full matrices electromechanical constants of $Ca_2Ga_2SiO_7$ and $Ca_2MgSi_2O_7$, and compared with $CaNdGa_3O_7$ (Ref. 18) crystals, from which the dielectric constant $\varepsilon_{11}^T/\varepsilon_0$ and piezoelectric coefficient d_{14} were found to be 11.7–16.8 and 5.3–9.3 pC/N, respectively.

The piezoelectric coefficient d_{14} of melilite crystals was thought to be attributed to the distortion (in *YZ*-plane) of the relatively soft eight-fold antiprisms, while d_{36} mainly comes from the distortion/rotation (in *XY*-plane) of the rigid tetrahedral layers.[18] In order to verify this hypothesis and further explore the piezoelectric origin, some structural parameters, including ionic radius, bond length, the ratio of bond length to ionic radius in eight-fold antiprisms, and piezoelectric coefficients are summarized in Table II.

For $Ca_2Ga_2SiO_7$ and $Ca_2MgSi_2O_7$, they have same CaO_8 antiprisms and similar d_{14} values, but different tetrahedrons and coefficients of d_{36}, hence, d_{36} mainly comes from the distortion/rotation of the tetrahedral layers. For $CaNdGa_3O_7$ and $Ca_2Ga_2SiO_7$ crystals, they have similar d_{36} values and same GaO_4 regular tetrahedrons but different irregular tetrahedrons, so d_{36} most probably attributes to the distortion/rotation of the regular tetrahedrons. From the aspect of microstructure, the corner linking of the irregular tetrahedrons restricts the rotation patterns,[19] so the distortion/rotation of regular tetrahedrons is easier than that of irregular ones under an applied electric field along the *Z*-direction, which also confirms that the piezoelectric d_{36} is originated from the distortion/rotation of the regular tetrahedrons.

As discussed previously, $Ca_2Ga_2SiO_7$ and $Ca_2MgSi_2O_7$ have same CaO_8 antiprisms and similar d_{14} values, while $CaNdGa_3O_7$ crystals possess different antiprisms and larger piezoelectric d_{14}, so d_{14} most probably attributes to the distortion of eight-fold antiprisms. In eight-fold antiprisms of the three melilite crystals, a larger bond length and/or a larger ratio of bond length to ionic radius indicates a larger space between the cation and oxygen ion, leading to "soft" antiprism (larger deformation) under applied electric field, accounting for the larger value of d_{14}.

D. Temperature dependent electrical resistivity

Figure 6 illustrates the dc electrical resistivity versus temperature for $CaNdGa_3O_7$, $Ca_2Ga_2SiO_7$, and $Ca_2MgSi_2O_7$, exhibiting the expected linear Arrhenius behavior. According to the Arrhenius equation, the activation energies (E_a) along *X*- and *Z*-directions can be calculated from the slope of the curves and were found to be in the range of 0.78–1.31 eV, related to the conductivity of the oxygen vacancies. It is interesting to note that the magnitude of the resistivity follows the trend of $Ca_2MgSi_2O_7 > Ca_2Ga_2SiO_7 > CaNdGa_3O_7$, which can be explained by the following two factors:

(1) The layered crystal structure: The tetrahedral layers interconnected by the large A site cations are vertical to the *Z*-direction, acting as barriers against charge

TABLE II. The structure and piezoelectric properties of melilite-type $CaNdGa_3O_7$, $Ca_2Ga_2SiO_7$, and $Ca_2MgSi_2O_7$ crystals.

			$CaNdGa_3O_7$	$Ca_2Ga_2SiO_7$	$Ca_2MgSi_2O_7$
In layers	Regular tetrahedron	Category	GaO_4	GaO_4	MgO_4
		Ion radius (Å)	0.47	0.47	0.57
		Bond length (Å)	1.827	1.821	1.921
	Irregular tetrahedron	Category	GaO_4	GaO_4/SiO_4	SiO_4
		Ion radius (Å)	0.47	0.47/0.26	0.26
		Bond length (Å)	1.785	1.737	1.629
Between layers	Eight-fold antiprism	Category	CaO_8/NdO_8	CaO_8	CaO_8
		Average bond length (Å)	2.598	2.581	2.568
		Ratio	2.331	2.304	2.293
Piezoelectric coefficient (pC/N)		d_{14}	9.3	6.4	5.3
		d_{36}	1.7	1.4	4.3

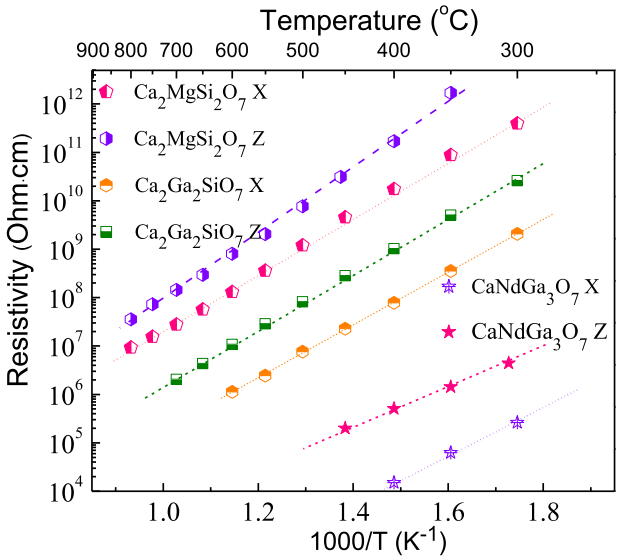

FIG. 6. Temperature dependent electrical resistivity of $CaNdGa_3O_7$, $Ca_2Ga_2SiO_7$, and $Ca_2MgSi_2O_7$ crystals.

transport.[20,21] The bond lengths of the eight-fold anti-prisms follow the trend of $Ca_2MgSi_2O_7 < Ca_2Ga_2SiO_7 < CaNdGa_3O_7$, where the shorter bond length means shorter distance between layers, resulting in a higher resistivity. This will also explain the higher resistivity along the *Z*-direction when compared to that along *X*-direction, as observed for all three crystals.

(2) The disordered structure: In the structure of $CaNdGa_3O_7$, Ca^{2+} and Nd^{3+} are distributed randomly with a ratio of 1:1 in eight coordinated sites, whereas in $Ca_2Ga_2SiO_7$, Si^{4+} and half of Ga^{3+} are distributed randomly in the irregular tetrahedral sites. It was reported that a high disorder level would induce phonon scattering, decreasing the electrical resistivity in disordered langasite-type piezoelectric crystals.[22] Analogous to this, the lower resistivity observed in $CaNdGa_3O_7$ crystals maybe related to the disordered structure (due to the similar ionic radii, $r^{Ca}(2+) = 1.12$ Å and $r^{Nd}(3+) = 1.11$ Å).[23] Similarly, the structure in $Ca_2Ga_2SiO_7$ gives rise to higher resistivity than that of $CaNdGa_3O_7$ (due to the large difference of ionic radii $r^{Ga}(4+) = 0.47$ Å and $r^{Si}(4+) = 0.26$ Å),[23] but lower than that of $Ca_2MgSi_2O_7$.

E. Temperature dependent dielectric and piezoelectric properties

Figure 7 presents the dielectric behaviors measured at 100 kHz as a function of temperature for $CaNdGa_3O_7$, $Ca_2Ga_2SiO_7$, and $Ca_2MgSi_2O_7$ crystals. As observed in the inset of Figure 7(a), the relative permittivity $\varepsilon_{11}^T/\varepsilon_0$ of $CaNdGa_3O_7$ was found to increase markedly over the temperature range of 25–300 °C, whereas the relative permittivities of the other two crystals increase slightly over the range of 25–500 °C. From Figure 7(a), all temperature coefficients of permittivity (TCε) were found to be positive, which can be explained based on the value of dielectric permittivity and dielectric loss using the modified Clausius-Mosotti equation[24,25]

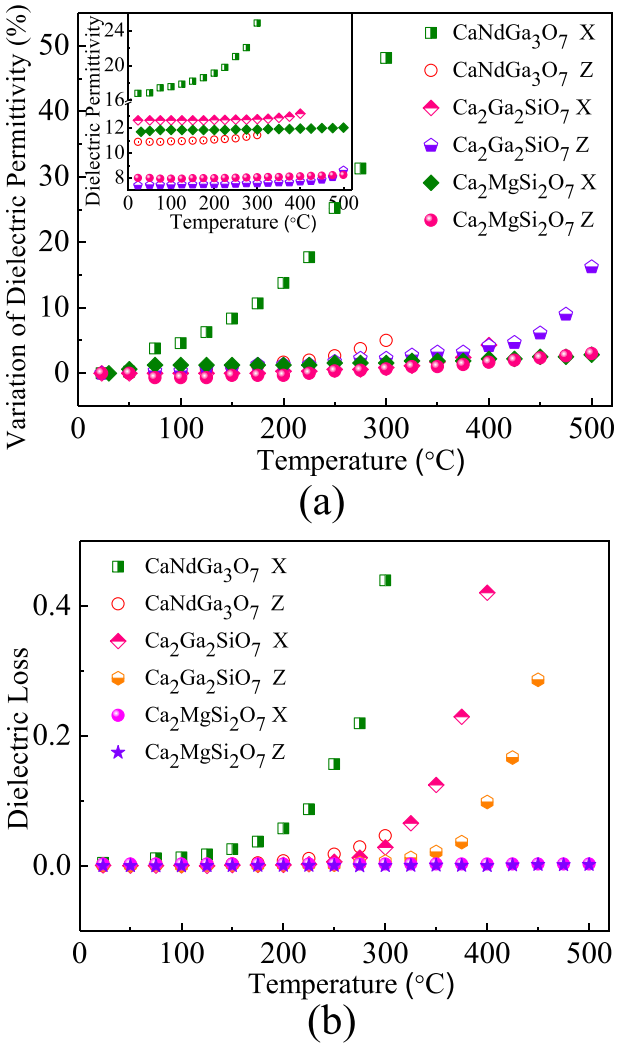

FIG. 7. The dielectric behaviors as a function of temperature for $CaNdGa_3O_7$, $Ca_2Ga_2SiO_7$, and $Ca_2MgSi_2O_7$ crystals along *X*- and *Z*-axes.

$$TC\varepsilon = \frac{(\varepsilon-1)(\varepsilon+2)}{\varepsilon}(A+B+C) + 0.05\tan\delta, \quad (1)$$

where $(A+B)$ indicates the effect of volume expansion with increasing temperature; C corresponds to the temperature dependence of the polarizability of the intrinsic ions and electrons with constant volume.[24,25] For materials with relative permittivities of $2.5 < \varepsilon_{ii}/\varepsilon_0 < 10$, ionic and electronic polarizability are comparable, and the TCε possesses a negative value if electronic polarizability dominating, and a positive value if ionic polarizability dominating, so the positive TCε of $Ca_2Ga_2SiO_7$ and $Ca_2MgSi_2O_7$ crystals with $2.5 < \varepsilon_{33}/\varepsilon_0 < 10$ was dominated by the ionic polarizability. For materials with relative permittivities $\varepsilon_{33}/\varepsilon_0 \geq 10$, TCε can be evaluated from the simplified equation

$$TC\varepsilon = \text{Constant-}\alpha\varepsilon, \quad (2)$$

where α is the linear thermal expansion coefficient. TCε decreased with increasing dielectric permittivity and shifts negatively when permittivity increased to beyond a certain value.[24,25] For materials with relative permittivities $\varepsilon_{33}/\varepsilon_0 \geq 10$ and high dielectric loss $\tan\delta > 0.1\%$, the TCε was dominated

by dielectric loss and can be calculated by the following formula:[24,25]

$$TC\varepsilon = 0.05 \tan \delta\text{-}\alpha\varepsilon. \quad (3)$$

As can be seen from Figure 7(b), the dielectric loss was observed to increase significantly at 250 °C for $CaNdGa_3O_7$ and at 300 °C for $Ca_2Ga_2SiO_7$, respectively, resulting in a remarkable increase in TCε over the studied temperature range. The high dielectric loss was believed to be related to their high ionic conductivity (low resistivity) at elevated temperatures.

Figure 8 presents the elastic constants as a function of temperature for $Ca_2Ga_2SiO_7$ and $Ca_2MgSi_2O_7$ crystals. From which, the diagonal components increase slightly with increasing temperature up to 500 °C, while the off diagonal elastic constants showing opposite tendency, decrease slightly over the studied temperature range. Both crystals exhibit high thermal stability of elastic constant over the range of 25–500 °C with minimal variation of 6%.

Piezoelectric coefficients as a function of temperature for $Ca_2Ga_2SiO_7$ and $Ca_2MgSi_2O_7$ crystals were determined, and compared with those of $CaNdGa_3O_7$, as given in Figure 9. For $CaNdGa_3O_7$, d_{14} maintained similar values over the temperature range of 25–400 °C, while d_{36} is decreased slightly from 1.7 pC/N to 1.1 pC/N over the range of 25–300 °C. Above these temperature ranges, the piezoelectric properties cannot be determined by impedance method, due to their low resistivity at elevated temperatures.

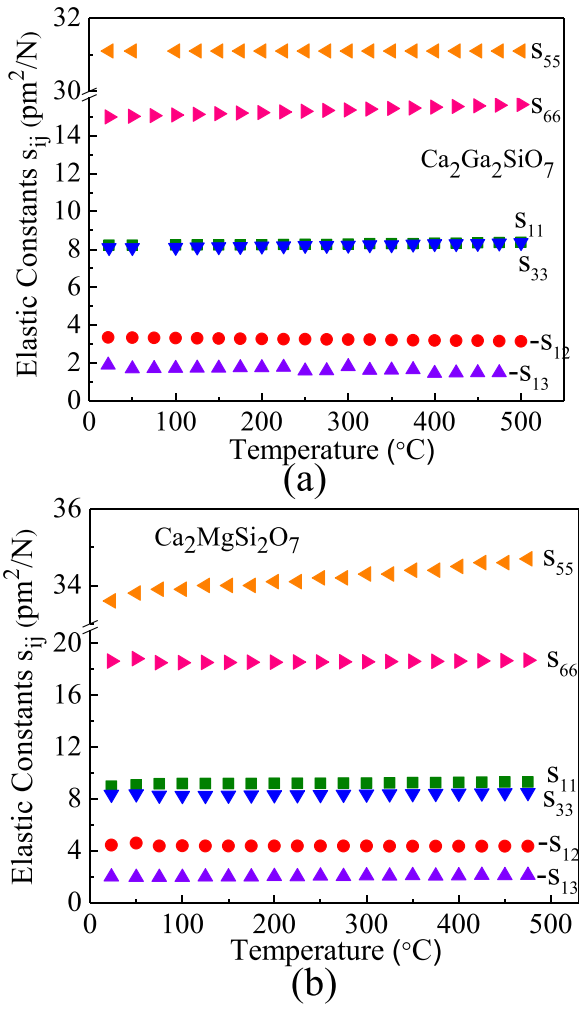

FIG. 8. The elastic constants as a function of temperature for $Ca_2Ga_2SiO_7$ and $Ca_2MgSi_2O_7$ crystals.

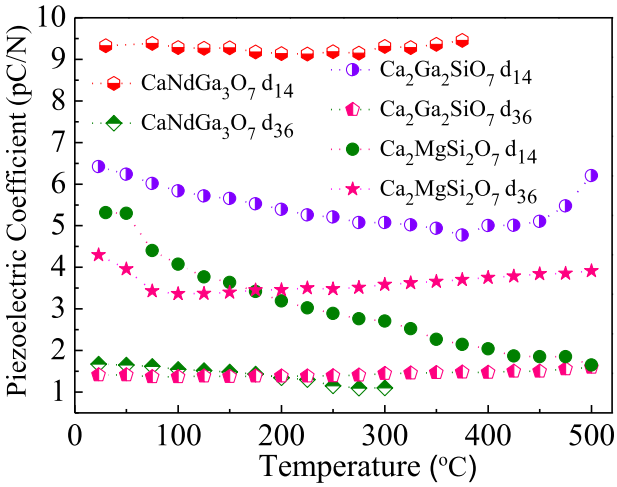

FIG. 9. Piezoelectric coefficients as a function of temperature for $CaNdGa_3O_7$, $Ca_2Ga_2SiO_7$, and $Ca_2MgSi_2O_7$ crystals.

For $Ca_2Ga_2SiO_7$, the value of d_{14} is decreased from 6.4 pC/N to 4.8 pC/N in the range of 25–375 °C, above which, the value is increased slightly to 6.2 pC/N at 500 °C. The increase in d_{14} above 375 °C is associated with the remarkable increase in dielectric permittivity ε_{11}^T. On the other hand, for $Ca_2MgSi_2O_7$ crystals, d_{14} is decreased from 5.3 pC/N to 1.7 pC/N with temperature increasing from 25 °C to 500 °C. The bond lengths of Ca-O were reported to increase with increasing temperature, with different variation levels for different Ca-O bonds,[26] leading to a certain degree of tilt for CaO_8 antiprisms, which may account for the decreased d_{14}. Piezoelectric coefficient d_{36} was found to decrease prior to the incommensurate-normal phase transition point $T_{ic\text{-}N}$, above which, it is increased. This can be explained by the distortion/rotation of the tetrahedral layers. In the structure of $Ca_2MgSi_2O_7$, the mean Ca-O bond length of 2.568 Å is larger than the typical Ca-O bond length of 2.500 Å calculated by ionic radii at room temperature. The trend to form adequate interstices for the Ca-ions is believed to be the driving force of the distortion/rotation of tetrahedrons.[19] Thus, the longer bond length of Ca-O, the larger the distortion/rotation of tetrahedrons, giving rise to larger d_{36} value. It should be noted that some of the Ca-O bond lengths in $Ca_2MgSi_2O_7$ are decreased from room temperature to $T_{Ic\text{-}N}$,[26] leading to the decreased d_{36} value. Above $T_{Ic\text{-}N}$, all the Ca-O lengths are increased with temperature,[26] thus d_{36} is increased slightly from 87 to 500 °C.

IV. CONCLUSIONS

$Ca_2Ga_2SiO_7$, $Ca_2MgSi_2O_7$, and $CaNdGa_3O_7$ single crystals with melilite structure were grown by the Czochralski method. Thermal properties, including thermal expansion and specific heat, were investigated. Full matrices of electromechanical constants of these melilite crystals were

measured by the impedance method with d_{14} being on the order of 5.3–9.3 pC/N. The relationship between microstructure and electromechanical properties of CNG, CGS, and CMS was established, which will benefit the exploration of the piezoelectric origin in melilite crystals. The distortion of eight-fold antiprisms and the distortion/rotation of tetrahedrons contribute to the piezoelectric coefficients d_{14} and d_{36}, respectively. In addition, the tetrahedral layers act as barriers against charge transport, leading to the highest resistivity in Z-cut $Ca_2MgSi_2O_7$ crystals, while a high disorder level induces phonon scattering and decreases the electrical resistivity, accounting for the degraded resistivity in $CaNdGa_3O_7$ crystals. The temperature dependence of properties was investigated, where the elastic constants showing a high thermal stability over the temperature of 25–500 °C with minimal variation of 6%.

ACKNOWLEDGMENTS

The authors would like to thank Professor Thomas R. Shrout for his helpful discussion. The authors from Shandong University acknowledged the National Natural Science Foundation of China (Grant No. 51372189).

[1]W. A. Deer, R. A. Howie, and J. Zussman, *An Introduction to the Rock-Forming Minerals*, 2nd ed. (Longman, London, 1992).
[2]M. Merlin, M. Gemmi, and G. Artioli, Phys. Chem. Miner. **32**, 189 (2005).
[3]A. Sugimoto, Y. Nobe, T. Yamazaki, Y. Anzai, K. Yamagishi, Y. Segawa, and H. Takei, Phys. Chem. Miner. **24**, 326 (1997).
[4]A. A. Kaminskii, L. Bohatý, P. Becker, J. Liebertz, P. Held, H. J. Eichler, H. Rhee, and J. Hanuza, Laser Phys. Lett. **5**, 845 (2008).
[5]Y. I. Sigalovskaya, Y. Z. Nozik, and A. B. Tovbis, Kristallografiya **34**, 316 (1989).
[6]S. F. Bartram, Acta Crystallogr., Sect. B **25**, 791 (1967).
[7]B. E. Warren, Z. Kristallogr. **74**, 131 (1930).
[8]J. V. Smith, Am. Mineral. **38**, 643 (1953).
[9]L. Bindi, P. Bonazzi, M. Dusek, V. Petricek, and G. Chapuis, Acta Crystallogr., Sect. B **57**, 739 (2001).
[10]L. Bohatý and J. Liebertz, Z. Kristallogr. **159**, 277 (1982).
[11]H. Takeda, M. Hagiwara, H. Noguchi, T. Hoshina, and T. Takahashi, Appl. Phys. Lett. **102**, 242907 (2013).
[12]M. Hiroaki, H. Noguchi, T. Hoshina, H. Takeda, S. Fujihara, N. Kodama, and T. Tsurumi, Jpn. J. Appl. Phys. Part 1 **52**, 09KD03 (2013).
[13]Y. Y. Zhang, X. Yin, H. H. Yu, H. J. Cong, H. J. Zhang, J. Y. Wang, and R. I. Boughton, Cryst. Growth Des. **12**, 622 (2011).
[14]C. Y. Shen, H. J. Zhang, Y. Y. Zhang, J. W. Wang, S. J. Zhang, and T. R. Shrout, in *2014 Joint IEEE International Symposium on the Applications of Ferroelectrics, International Workshop on Acoustic Transduction Materials and Devices & Workshop on Piezoresponse Force Microscopy (ISAF/IWATMD/PFM)* (IEEE, 2014), pp. 195–198.
[15]IEEE Standard on Piezoelectricity, ANSI/IEEE Std 176-1987, American Standards National Institute, New York, 1987.
[16]K. Iishi, T. Mizota, K. Fujino, and Y. Furukawa, Phys. Chem. Miner. **17**, 720 (1991).
[17]S. L. Webb, C. R. Ross II, and J. Liebertz, Phys. Chem. Miner. **18**, 522 (1992).
[18]C. Y. Shen, S. J. Zhang, D. L. Wang, T. X. Xu, H. H. Yu, W. W. Cao, J. Y. Wang, and H. J. Zhang, CrystEngComm **17**, 1791 (2015).
[19]C. V. Heurck, G. V. Tendeloo, and S. Amelinckx, Phys. Chem. Miner. **18**, 441 (1992).
[20]M. Miyayama and I. S. Yi, Ceram. Int. **26**, 529 (2000).
[21]C. Y. Shen, H. J. Zhang, H. J. Cong, H. H. Yu, J. Y. Wang, and S. J. Zhang, J. Appl. Phys **116**, 044106 (2014).
[22]S. J. Zhang and F. P. Yu, J. Am. Ceram. Soc. **94**, 3153 (2011).
[23]R. D. Shannon, Acta Crystallogr., Sect. A **32**, 751 (1976).
[24]A. G. Cockbain and P. J. Harrop, J. Phys. D **1**, 1109 (1968).
[25]D. K. Kwon, Ph. D. dissertation, Materials Science and Engineering Department, The Pennsylvania State University, 2006.
[26]K. Kusaka, K. Hagiya, M. Ohmasa, Y. Okano, M. Mukai, K. Iishi, and N. Haga, Phys. Chem. Miner. **28**, 150 (2001).